



Numerical simulation of dynamic catastrophe of slope instability in three Gorges reservoir area based on FEM and SPH method

Zhengyang Su¹ · Guizhi Wang² · Yakun Wang³ · Xiang Luo¹ · Hao Zhang¹

Received: 24 June 2021 / Accepted: 1 October 2021 / Published online: 18 October 2021
© The Author(s), under exclusive licence to Springer Nature B.V. 2021

Abstract

Affected by continuous heavy rainfall, a large number of landslide disasters occur every year in the Three Gorges Reservoir area, which causes serious property loss and casualties. In this study, we take a typical reservoir slope as an example. Firstly, the change of plastic zone of the slope under the action of continuous heavy rainfall before the failure is simulated based on the FEM method, considering the coupling of seepage field and stress field. Then, based on the smooth particle hydrodynamics method, HBP rheological model and Drucker–Prager yield criterion are used to simulate the dynamic catastrophic process of slope sliding after instability, and the time–space distribution of velocity field and accumulation form of the landslide are obtained based on the N-S equation. By analyzing the erosion behavior at the junction of various materials on the slope, the dynamic mechanism of the slope instability and slippage is revealed.

Keywords Three Gorges reservoir slope · Continuous heavy rainfall · Flow-slip process · FEM · SPH · HBP constitutive model

1 Introduction

Rapid change of climate and environment (Boyages 2013), has led to the rampant formation of several landslides (Wang and Zhang, 2021; Xu et al. 2021), severe floods (Rangari et al. 2021), and also debris flow (Li et al. 2019a, b). These formations have caused extreme loss of lives and properties. Three Gorges Dam in China is the world’s largest hydroelectric project (Keqiang et al. 2008). The dam is 185 m high, 2.3 km long with an average water level that fluctuates between 145 and 175 m, respectively. Due to the heavy

✉ Zhengyang Su
zysunhri@163.com

¹ State Key Laboratory of Hydrology-Water Resources and Hydraulic Engineering, Nanjing Hydraulic Research Institute, Nanjing Jiangsu 210029, China

² Jiangsu Water Conservancy Survey, Design and Research Institute Co. Ltd, Yangzhou Jiangsu 225009, China

³ Hohai University, Nanjing Jiangsu 210098, China

rainfall, the reservoir water level changes (Zhang et al. 2019, 2020), which has led to the consistency in the increase in the formation of reservoir landslides (Wang et al. 2019; Tang et al. 2020), which seriously threatens the safety of people's lives and property.

Due to the heavy rainfall, the soil on the surface of the slope gradually changes from unsaturated to saturated which decreases the soil's strength parameters thereby begetting landslides and other natural disasters (Xing et al. 2021). Also, the rainfall scouring effect occurs as the rainfall continues while the soil is already saturated, soil and rainwater are mixed to form mud. Again the local plastic zone of slope develops continuously, which gradually develops into disasters such as landslides and debris flows (Pastor et al. 2010), causing severe instabilities. Landslides can be effectively controlled and prevented by having an in-depth understanding of certain parameters such as the process of dynamic instability and siltation, the temporal and spatial distribution of the landslide flow velocity field, and accumulation pattern. The former mainly affects the impact force and dynamic response of landslide flow to the prevention and control of engineering structure, while the latter is of great significance to the analysis of landslide flow scope and hazard assessment. Currently, a combination of field survey and remote sensing technology is the most effective carried out field investigations methodology to study the incitation conditions and erosion process of a runoff-triggered debris flow in Miyun County, Beijing, China. (Ma et al. 2018). Kaya et al. (2020) Studied a landslide case in the eastern part of the Black Sea in northeast Turkey on the cause and mechanism of landslide sliding by drilling, geophysical survey, and inclinometer measuring method, and relevant measures were put in place to prevent landslide. Askarinejad et al. (2018) experimented on a natural sandy slope subjected to an artificial rainfall event. Here novel slope deformation sensors were applied to monitor the subsurface pre-failure movements. Xiong et al. (2021) studied the activity characteristics and enlightenment of the debris flow triggered by the rainstorm in Wenchuan County, China. It was then stipulated although field investigation and field are extremely cost-effective. There is still exitance some failures such instrument failure or incomplete information gathered. For example, Bondur et al. (2019) used L-band radar interferometric observations to monitor the collapse and landslide process of the Brea River. It was concluded that summer images were less informative because of the abrupt loss of coherence in the case of heavy precipitation. Therefore, due to the uncertainty and complexity of the landslide flow, the traditional methods such as field prototype observation and model test have indicated several limitations but numerical simulation based on physical processes provides an effective means to study and analyze the above problems. According to the domain discretization analysis, the existing landslide numerical models can be divided into two types: grid method and mesh-free method. In the grid method, the computational domain is discretized by continuous and fixed grid elements. It is solved by finite difference method (FDM), finite element method (FEM), finite volume method (FVM), or other numerical methods. The Grid method has been widely used in numerical simulation of landslides. Based on the finite element method, Yu et al. (2020) calculated the seepage, stability, and deformation characteristics of a slope in the Three Gorges reservoir area with regards to underwater level fluctuations while taking into account the influence of anisotropy ratio and anisotropy direction. Zhang et al. (2020) used the finite difference method to analyze the plastic zone, safety factor, and stability of the landslide in the Three Gorges Reservoir area, per measured slope displacement data and recommended drawdown of the water level in the reservoir by careful control to mitigate the landslide mass effect. However, restricted by the grid itself, the grid method still has many challenges in dealing with complex grid structures, complex boundaries, free surfaces, and large deformations (Yu et al. 2021).

Due to continuous heavy rainfall, the slope soil is constantly eroded, which has shown similar fluid properties. Given the grid method limitations, the mesh-free method a discontinuous medium model has gradually been applied to the numerical simulation of landslide flow. Typical mesh-free methods include discrete element method (DEM) (Zhu et al. 2020), discontinuous deformation analysis (DDA) (Hwang et al. 2004), moving particle method (MPS) (Koshizuka et al. 2015), the material point method (MPM) (Sulsky et al. 1994) and Smoothing Particle Hydrodynamics (SPH) (Lucy 1977; Liu et al. 2008). DEM is mostly suitable for particle sorting, start-up mechanism research, and simulation of water–rock flow and debris flow with low viscosity (Kwok and Bolton 2013). DDA has been widely used in the fields of rockfall, landslide, and debris flow movement analysis (Hwang et al. 2004). These two methods reflect little information on unique complex fluid characteristics of debris flow. It reveals low outcomes when applied to landslide flow simulation. Recently, substantial progress has been made using meshless methods, such as MPM (Soga et al. 2016; Li et al. 2018), SPH, (Bui et al. 2010; Huang et al. 2013; Pastor et al. 2014), and MPS (Huang and Zhu 2014; Nohara et al. 2018; Zhu et al. 2021). SPH method is based on particle and kernel function to discretize and solve the governing equations in the computational domain. SPH method has good applicability in the numerical simulation of a flood, debris flow, and other fluid media because of its particle characteristics, and ease to describe the constitutive relationship of different materials. Compared with SPH and MPS, MPM requires a background grid system to solve the momentum equations. Regarding the SPH applications on landslide propagation, Pastor et al. (2014) proposed an improvement, based on combining Finite Difference meshes associated with SPH nodes to describe pore pressure evolution inside the landslide mass. Follow-up research depicted that, the depth integration model is continuously developed and applied to the modeling of landslide propagation (Pastor et al. 2015a, b; Tayyebi et al. 2021). Liang and Wang (2020) proposed a displacement-based criterion to locate the failure slip surfaces based on the smooth particle hydrodynamics method. Dai et al. (2020) established two-dimensional and three-dimensional models of debris flow in Tibet, China, using the SPH method to analyze the dynamic characteristics of debris flow such as velocity, jumping distance, deposition, and energy characteristics.

Another key problem in numerical simulation of landslide flow is the description of its rheological properties. Pastor et al. (2015a, b) propose an alternative rheological model based on Perzyna's viscoplasticity. Manzanal et al. (2016) presented a depth-integrated SPH model, which can be used to simulate real rock avalanches and also to assess the influence of rheology on the avalanche properties. Brezzi et al. (2016) presented a numerical procedure based on the application of a statistical algorithm to develop a debris flow run-out model. Existing studies have confirmed that when the shear deformation of landslide and debris flow is large, the multiphase mixture of soil, sand, and water with different proportions has shear thickening or shear thinning behavior, which is suitable to be described by Herschel–Bulkley (HB) model large (Shen et al. 2019; Ouyang et al. 2019). Calvo et al. (2015) analyzed the influence of the uncertainties related to initial volume and initial mass morphology (using the aspect ratio as a parameter) on the spreading of Bingham fluid. However, the HB model is essentially a derivative of the Bingham model, and there is still a problem of numerical divergence when it is transformed into an equivalent viscosity coefficient. Papanastasiou (1987) proposed an HB-Papanastasiou (HBP) model which approximates the HB model with a continuous function while Frigaard and Nouar (2005) further confirmed its applicability in subsequent studies.

In this study, the Three Gorges reservoir slope is taken as a case study. Firstly, seepage field and stress field coupling is examined, while the change of plastic zone of the

slope before failure under continuous heavy rainfall is simulated by the finite element method. HBP rheological model and Drucker–Prager yield criterion are used to simulate the dynamic catastrophic process of landslide on the slope after instabilities. Then the smoothed particle hydrodynamics method is applied to estimate the temporal and spatial distribution and accumulation state of the landslide velocity field. Finally, the dynamic mechanism of the slope instability and slippage is calculated by analyzing the erosion behavior at the interface of various materials on the slope.

2 The theory of calculation

2.1 Saturated–unsaturated seepage theory

According to Darcy’s law of unsaturated soil and the seepage continuity equation of porous media, the saturated–unsaturated differential equation expressed by pressure head can be obtained as follows:

$$\frac{\partial}{\partial x_i} \left[k_{ij}^s k_r(h_c) \frac{\partial h_c}{\partial x_j} + k_{i3} k_r(h_c) \right] + Q = \left[C(h_c) + \frac{\theta}{n} S_s \right] \frac{\partial h_c}{\partial t} \quad (1)$$

where k_{ij}^s is the saturation permeability tensor; k_r is the relative permeability; h_c is the pressure head; Q^* is the source and sink term; $C(h_c)$ is the water capacity, n is the porosity; and S_s is the unit water storage.

2.2 Basic theory of SPH

SPH method discretizes the computational domain with discrete particles, and the physical quantity of each particle is determined by the interpolation sum of adjacent particles based on kernel function. In SPH method, every element point is called base point, on which all calculation parameters and result information are recorded. We use the continuity equation (Zhu et al. 2018)

$$\frac{d\rho_i}{dt} = \sum_{j=1}^N m_j v_{ij}^\beta \frac{\partial W_{ij,\beta}}{\partial x_i^\beta} \quad (2)$$

and the momentum equation

$$\frac{dv_i^\alpha}{dt} = \sum_{j=1}^N m_j \left(\frac{\sigma_i^{\alpha\beta}}{\rho_i^2} + \frac{\sigma_j^{\alpha\beta}}{\rho_j^2} + T_{ij} \right) \frac{\partial W_{ij,\beta}}{\partial x_i^\beta} \quad (3)$$

where: ρ is the base point density, kg/m^3 ; t is the calculation time, s; m is the mass, kg; v is the velocity of the base point, m/s ; x is the position coordinate of the base point, m; T is the artificial viscosity term to reduce the non-physical oscillation in the calculation process; W is the smooth kernel function of SPH.

In order to simplify the calculation process of the pressure term and improve the calculation efficiency, we used the weakly compressible SPH algorithm to solve the normal stress based on the equation of state.

$$P_i = \frac{c^2 \rho_0}{\gamma} \left[\left(\frac{\rho_i}{\rho_0} \right)^\gamma - 1 \right] \tag{4}$$

where: c is the speed of sound, calculated according to $c = \beta(g h_{max})^{1/2}$, β is taken as 10 in this article; ρ_0 is the reference density; γ is a constant value, usually taken as 7.

3 Numerical simulation

3.1 Project overview

The slope is located at the exit section of Qutang Gorge on the north bank of the Yangtze River, 148.3 km away from the Three Gorges Dam in the east, and 457 km away from Chongqing City. Figure 1 shows the slope’s geographical location. The slope is located in a subtropical monsoon climatic zone with an average annual temperature of 18.4 °C and an average annual rainfall of 1049.3 mm, respectively. Rainfall mainly occurs from May to October, with heavy rain from July to August, with maximum daily rainfall was 371.3 mm.

3.2 FEM numerical model

3.2.1 Numerical model and boundary conditions

The finite element model of the reservoir slope is shown in Fig. 2(a). Here analysis was made by setting certain parameters that are bedrock was modeled as a linear elastic material, the landslide mass was modeled as ideal elastic–plastic material, and also the contact zone between the landslide mass and the bedrock, which can be regarded as a

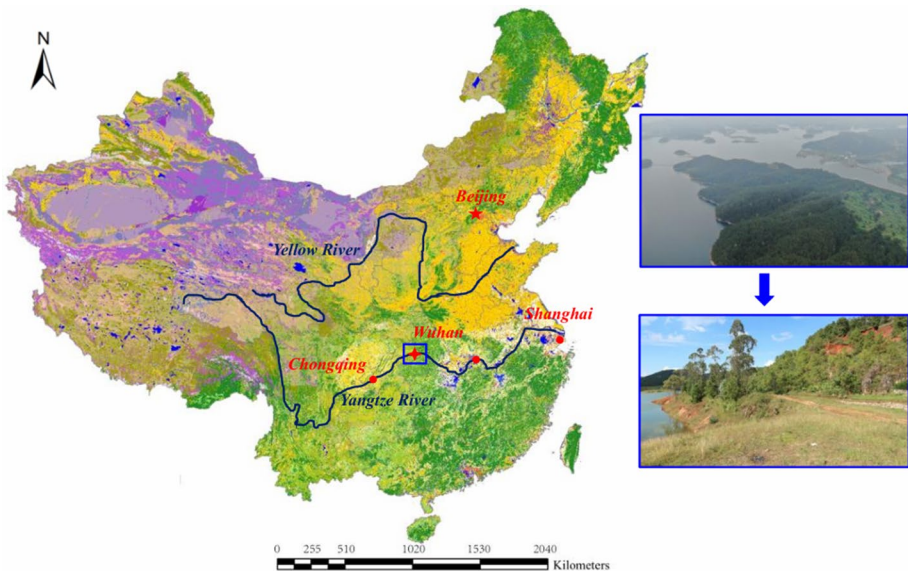


Fig. 1 Geographical location and basic overview of the slope (Chinese mainland)

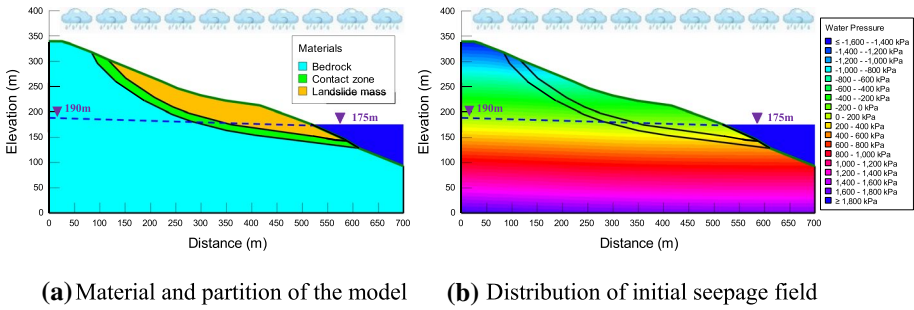


Fig. 2 Schematic diagram of finite element model

shear band was also modeled as ideal elastic–plastic material. It is assumed that the failure slope follows the Mohr–Coulomb criterion. Hydraulic boundary mainly includes reservoir water level boundary, groundwater level boundary and rainfall boundary. The seepage of groundwater level was considered in the model while the boundary of water levels was set at 145 m ~ 175 m. Figure 2(b) shows the distribution of pore water pressure of the slope when the water level is 175 m. The global element size of the finite element model was 0.5 m, and the model was divided into 16,158 nodes and 15,860 elements, respectively.

The soil–water characteristic curve of the slope soil is shown in Fig. 3, which is estimated by the infiltration model in the GeoStudio software, and the parameters of finite element calculation are shown in Table 1. The parameters were determined from the field tests. Considering the continuous rainfall condition, the unit flow boundary was used for rainfall simulation. The simulation of rainfall intensity was realized by defining different unit flow boundary functions. In the numerical simulation, the rainfall intensity was 30 mm/d, and the rainfall duration was set to 30 days. Rainfall stopped after 30 days while water level drops from 175 to 145 m, with variation rates set as 1 m/d, 2 m/d, and 3 m/d, respectively. The total calculation time is set to 60 days.

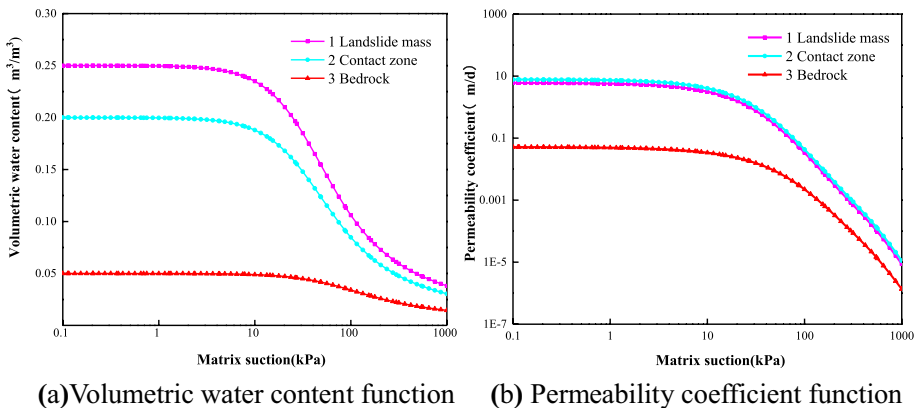


Fig. 3 Soil–water characteristic curve

Table 1 The main physical and mechanical parameters used in numerical calculation

Partition	Volume weight (kN/m ³)	osmotic coefficient (m/s)	water content (m ³ /m ³)	Internal friction angle (°)	Cohesion (MPa)	Modulus of elasticity (GPa)
Landslide mass	22.7	7×10^{-5}	0.25	15	16	0.85
Contact zone	21.7	9×10^{-5}	0.20	16	21	0.75
Bedrock	27.0	6×10^{-6}	0.05	20	24	4.00

3.2.2 Distribution characteristics of plastic zone

The failure mechanism of the reservoir slope under the influence of rainfall and water level fluctuation, the development characteristics of an identical plastic zone of the slope under the most dangerous condition were examined to reveal the progressive failure mechanism of the slope. During the continuous rainfall, the rainfall intensity was 30 mm/d, the water level dropped at a rate of 3 m/d, and the development characteristics of the equivalent plastic zone of the slope are shown in Fig. 4. Here it can be seen that in the initial stage, under the combined action of water load pressure and seepage force, a large area of plastic zone appears in the leading edge of the slope. Therefore, rainfall directly changed the distribution of seepage fields on the surface of the soil. The surface soil of the slope gradually turns to be saturated thereby reducing the shear strength of the soil while the surface soil of the slope enters the yield stage.

In the numerical simulation, three variation rates of water level are selected to study the influence of the velocity of reservoir level drop on landslides exhibiting instability. The

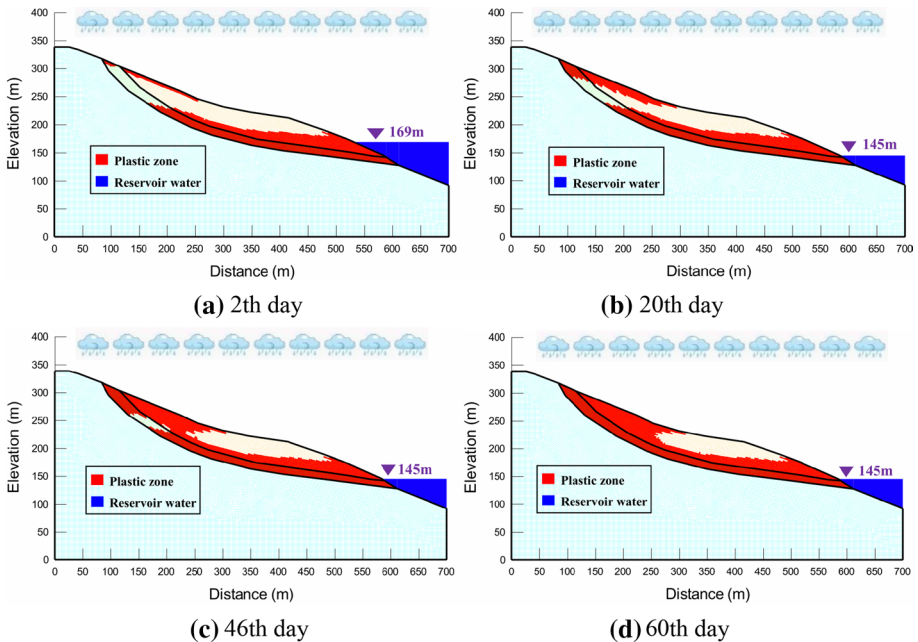


Fig. 4 The development of the plastic zone of the reservoir slope under the most dangerous conditions

numerical simulation results show that the main area affected by the water level drop is the front edge of the landslide, and the water level drop induces a local shallow landslide in the front edge of the landslide. When the water level drops rapidly, the decline of groundwater level lags behind the decline of water level, causing the excess pore water pressure and seepage force inside of the landslide to point in the outward direction of the landslide body. The generation of drag force pointing to the outside of the landslide mass is very unfavorable to the stability of the landslide mass. The seepage force is directly proportional to the hydraulic gradient. That means the faster the water level drops, the greater the hydraulic gradient along the slope, and also the greater the seepage force pointing to the outside of the landslide mass, and the worse the stability of the landslide mass.

As the rainfall continues, the water infiltrates into the slope, reducing the strength of the surface soil of the slope, and the plastic zone of the trailing edge of the slope is expanding as shown in (Fig. 4(b), (c)). The main influences of high-intensity rainfall on the slope are rain-drop splash erosion, slope runoff erosion, and rainfall loading. Under high-intensity rainfall conditions, the surface soil of the slope reaches a saturated state in a short time, but the soil of the slope has no time to dissipate the groundwater, which leads to high pore water pressure in the pores or fissures of rock and soil. Moreover, when the groundwater seeps into the lower part of the slope, hydrodynamic pressure (seepage pressure) will be generated inside the slope. Its direction is consistent with the seepage direction, which will also increase the sliding force of the reservoir slope and increases the possibility of slope instability.

In the final stage of destruction, the plastic zone of the reservoir slope starts to run through, and the plastic zone continues to develop to the interior of the slope. The slope has been damaged at this time, and the combined effect of rainfall and water level at this stage tends to induce severe landslides.

3.3 SPH numerical model

The traditional finite element method has limitations to deal with the problems related to large deformation. When compared with the grid-based method, the advantages of SPH include no need for grids, strong anti-distortion ability, ability to deal with large deformation, multi-scale and high-speed collisions, avoiding a large number of element divisions, and overcoming the error caused by local approximation of field function in finite element method. It can be used to calculate some difficult and complex problems that are not easy to examine with the grid method. Therefore, in this study, the SPH method is employed to simulate the large deformation movement of the slope after instability.

3.3.1 Constitutive model of landslide (HBP)

Herschel–Bulkley–Papanastasiou (HBP) model was used to model the rheological characteristics of mobile landslide. The HBP model and its equivalent viscosity coefficient are expressed as follows:

$$\tau_{ij} = \tau_y [1 - e^{-m\gamma}] + 2\mu (\epsilon^{\alpha\beta})^n \quad (5)$$

$$\mu_{\text{eff}} = \frac{|\tau_y|}{\gamma} [1 - e^{-m\gamma}] + 2\mu\gamma^{n-1} \quad (6)$$

where: γ is the shear strain rate; μ is the apparent dynamic viscosity; τ_y is the yield stress; m controls the exponential growth of stress, and n is a power-law exponent, which can simulate shear thinning or shear thickening. When $m=0$ and $n=1$, the model is simplified as Newton model, while when $m \rightarrow \infty$ and $N=1$, the model is simplified as Bingham model. The final SPH momentum equation is expressed as follows:

$$\frac{dv_i^\alpha}{dt} = - \sum_{j=1}^N m_j \left(\frac{\sigma_i^{\alpha\beta}}{\rho_i^2} + \frac{\sigma_j^{\alpha\beta}}{\rho_j^2} \right) \frac{\partial W_{ij}}{\partial x_i^\alpha} + \sum_{j=1}^N m_j \left(\frac{\mu_{\text{eff}i}^{\alpha\beta}}{\rho_i^2} + \frac{\mu_{\text{eff}j}^{\alpha\beta}}{\rho_j^2} \right) \frac{\partial W_{ij}}{\partial x_i^\beta} + g^\alpha \quad (7)$$

On the basis of smoothed particle hydrodynamics, HBP model is used to describe the rheological characteristics of landslide after instability, and the yield condition of landslide is judged based on DP criterion. In this paper, Drucker–Prager yield criterion is used. The general form of Drucker-Prager model is as follows:

$$f = \sqrt{J_2} + (\alpha p - \kappa) \quad (8)$$

where: J_2 is the second deviatoric stress invariant, α and κ can be determined by Mohr–Coulomb yield criterion:

$$\alpha = -\frac{2\sqrt{3} \sin \varphi}{3 - \sin \varphi}, \quad \kappa = -\frac{2\sqrt{3}c \cos \varphi}{3 - \sin \varphi} \quad (9)$$

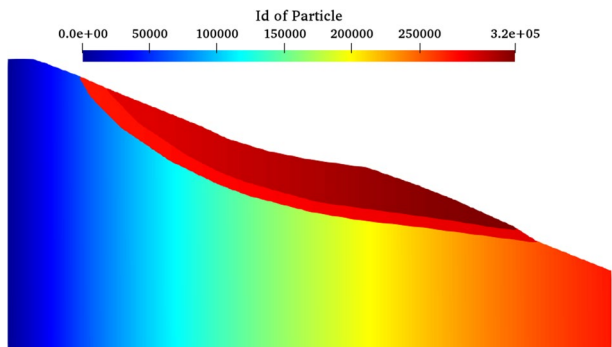
From Eq. (11) and $\sqrt{J_2} = 2\mu\gamma$, the erosion start condition expressed by the Drucker–Prager criterion can be:

$$-\alpha p + \kappa < 2\mu\gamma \quad (10)$$

3.3.2 Distribution of landslide particles

In this section, the SPH method is used to simulate the dynamic process of slope instability. The total number of particles in the numerical simulation is 320531, and the distribution of each particle ID is shown in Fig. 5. In the numerical simulation, the calculated interval at $\Delta t=0.01$ s, the number of interval steps is 600 with a total estimated time of 6 s. The no-slip boundary is adopted at the bottom and on both sides of the slope. The

Fig. 5 ID distribution of particles in SPH model



numerical model partition of reservoir slope is shown in Fig. 2. Here, the Verlet algorithm is chosen as the time-stepping algorithm. For landside mass area, $m=0$, $n=1$; for contact zone area, $m=100$, $n=1.5$; for bedrock area, $m=1000$, $n=2$.

3.3.3 Dynamic catastrophe process analysis

To examine the dynamic process of flow sliding after slope instability, the velocity field distribution, vorticity field distribution, and accumulation pattern distribution of slope under different calculation steps are shown in Figs. 6, 7, 8, 9, 10 and 11.

It can be seen from (Fig. 6) the distribution of velocity field that when $T=1$ s, the velocity at the leading edge and the trailing edge of the slope first increases, and the initial sliding velocity is about 3.5 m/s, which indicates that the leading and trailing edge of the slope begins to slide which shows the first stage of slope instability. Again, when $T=1.5$ s, the

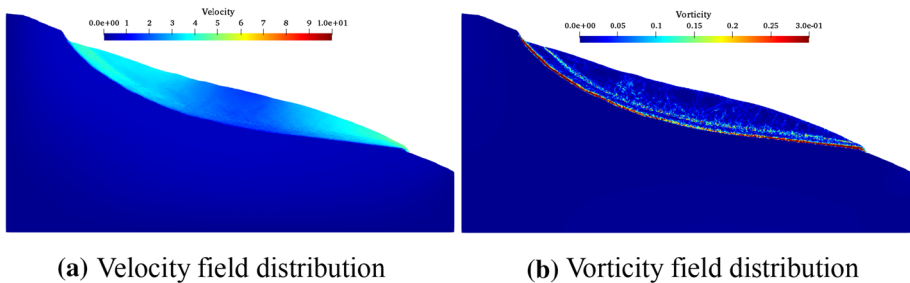


Fig. 6 Flow-slip characteristics of landslide at $T=1$ s

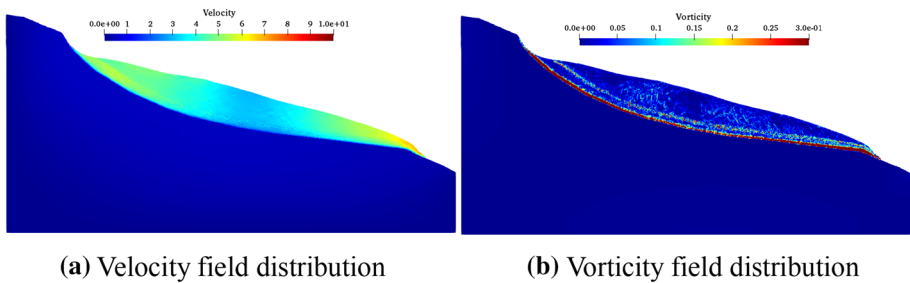


Fig. 7 Flow-slip characteristics of landslide at $T=1.5$ s

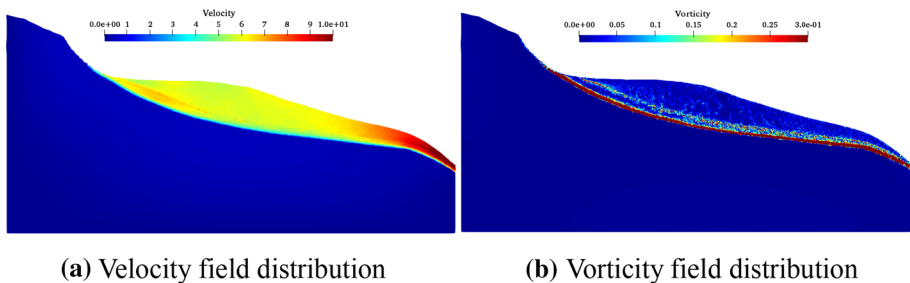


Fig. 8 Flow-slip characteristics of landslide at $T=2.5$ s

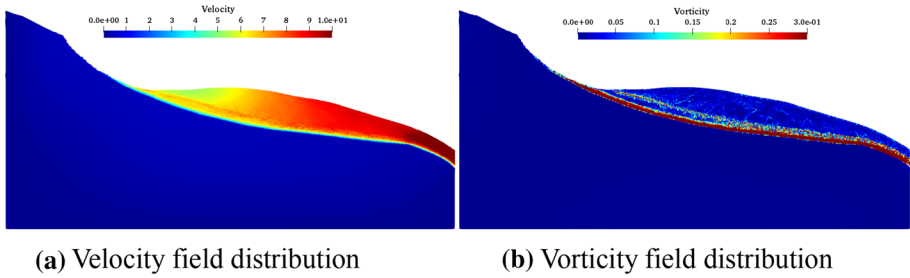


Fig. 9 Flow-slip characteristics of landslide at $T=3.5$ s

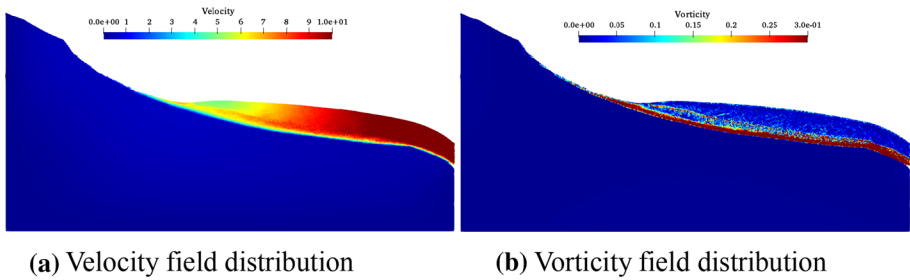


Fig. 10 Flow-slip characteristics of landslide at $T=4.5$ s

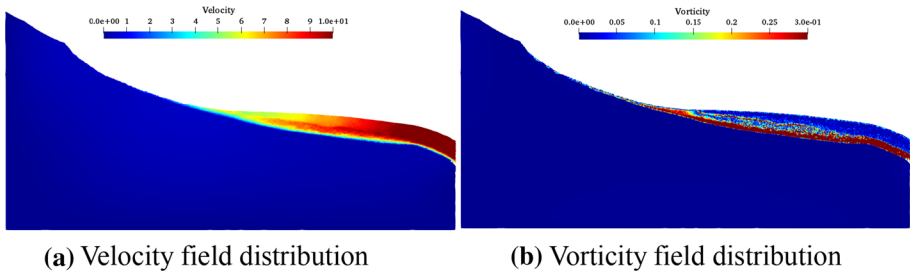


Fig. 11 Flow-slip characteristics of landslide at $T=6$ s

velocity of the leading edge and trailing edge of the slope continues to increase, and the sliding velocity of the leading edge is slightly higher than that of the trailing edge of the slope. The maximum sliding velocity of the leading edge of the slope reaches 6.5 m/s. Also, when $T=2.5$ s, the sliding speed of the front edge of the slope has reached 10 m/s, which indicates a continuous process of instability. The area of the slope sliding speed greater than 10 m/s gradually increases, which depicts that the slope is gradually showing a trend of overall sliding, and its velocity distribution is: the leading edge of the slope > middle part of the slope > trailing edge of the slope. Velocity is one of the key dynamic characteristics in the process of landslide flow propagation. Existing research shows that the sliding velocity of sliding mass is generally between 10 m/s and 100 m/s when landslide and debris flow occur (Li et al. 2019a, b; Kang et al. 2017; Dai et al. 2020), which indicates that the numerical simulation results in this paper are reasonable.

When the slope is unstable under the action of continuous rainfall and flow sliding occurs, the slope soil has already shown the properties of a fluid. In this study, the HBP

constitutive model is used to describe the rheological behavior of slope soil. Vorticity is mainly used to describe the rotation of landslides. From the distribution of vorticity field, when $T=1$ s, the vorticity at the interface of landslide mass and contact zone, the contact zone, and the bedrock material changes significantly. At this time, erosion has occurred at the boundary, and the erosion at the interface of contact zone and bedrock is more severe, with the maximum vorticity greater than 0.3. When $T=2.5$ s~6.0 s, the two erosion interfaces merge gradually.

3.3.4 Evolution of erosion surface

The typically saturated sediment scour caused by the rapid liquid flow at the interface has undergone many different behavior changes, which are mainly controlled by the characteristics of sediment and liquid rheology at the interface. These sediment regimes are distinguishable as an un-yielded region of sediment, a yielded non-Newtonian region, and a pseudo-Newtonian sediment suspension region where the sediment is entrained by the liquid flow. These physical processes can be described by the Coulomb shear stress τ_{mc} , the cohesive yield strength τ_c which accounts for the cohesive nature of fine sediment, the viscous shear stress τ_v which accounts for the fluid particle viscosity, the turbulent shear stress of the sediment particle τ_t and the dispersive stress τ_d which accounts for the collision of larger fraction granulate. The total shear stress can be expressed as:

$$\tau^{\alpha\beta} = \tau_{mc} + \tau_c + \tau_v^{\alpha\beta} + \tau_t^{\alpha\beta} + \tau_d^{\alpha\beta} \quad (11)$$

The first two parameters on the right-hand side of the equation define the yield strength of the material and thus can be used to differentiate the un-yielded or yielded region of the sediment state according to the induced stress by the liquid phase in the interface. In this study, the Drucker–Prager yield criterion was employed to evaluate the yield strength of the sediment phase and the sediment failure surface. When the material yields, the sediment behaves as non-Newtonian rate-dependent Bingham fluid that accounts for the viscous and turbulent effects of the total shear stress. Distinctively, sediment behaves as a shear-thinning material with a low and high shear stress state of a pseudo-Newtonian and plastic viscous regime, respectively.

By capturing the interface in the numerical simulation, the erosion phenomenon at the interface of various materials in the process of the landslide was simulated as shown in (Fig. 12). When continuous heavy rainfall causes the slope to slide, the leading edge and the trailing edge of the slope begin to slide first, and then the soil at the interface of the material appears to shear erosion. When sliding continues, it can be seen from Fig. 12 (e) (f) that more and more particles are taken away by erosion at the interface of materials. At the same time, the erosion phenomenon at the interface also shows that the erosion speed and area of the leading edge of the landslide are both greater than those of the trailing edge.

4 Conclusion

In this study, numerical simulations of the dynamic mutation process before and after the instability of the slope in the Three Gorges Reservoir area are carried out based on the FEM and SPH methods, and the conclusion is as follows.

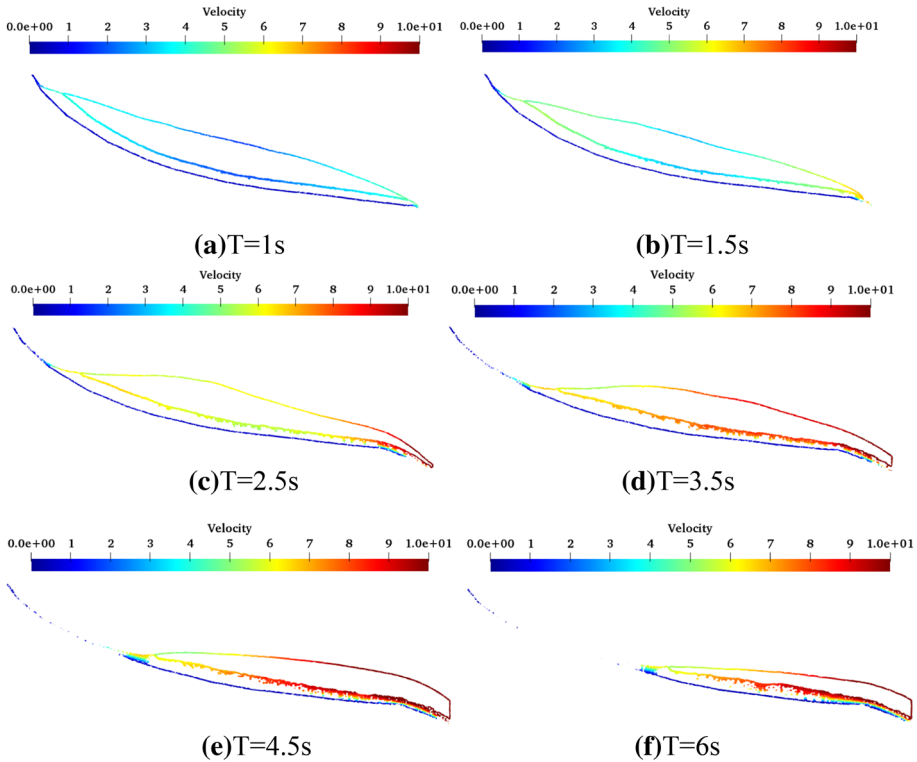


Fig. 12 Erosion process at the interface of slope materials

- (1) In the early stage of rainfall, part of the plastic zone appears in the surface soil of the slope, and a large area of plastic zone appears in the leading edge of the slope under the action of water level. When rainfall is continuous, the plastic zone at the trailing edge of the slope expands ceaselessly. When the plastic zone is connected, it is considered that the slope begins to slide. At this stage, the combined action of rainfall and water level easily induces deep landslide.
- (2) In the stages of slope instability and flow sliding under the action of heavy rainfall, the leading and trailing edge of the slope begins to slide first. The sliding velocity of the leading edge is slightly higher than that of the trailing edge of the slope, and the maximum sliding velocity of the leading edge of the slope reaches 10 m/s. Here the slope is gradually showing a trend of overall sliding, and the velocity distribution is the leading edge of the slope > middle part of the slope > trailing edge of the slope. In the process of landslide flow, shear erosion occurs at the interface of materials, then more and more particles are taken away by erosion at the interface of materials.
- (3) Under continuous heavy rainfall, the slope soil shows the flow property of the fluid, which can be simulated by the HBP model. FEM method is suitable for the simulation of the slope before instability, whereas the SPH method is suitable for the simulation of large deformation after instability. The combination of the FEM and SPH method can simulate the whole process of slope instability.

Acknowledgements The authors gratefully acknowledge the finances support provided by: National Natural Science Foundation of China (Key Program) [Grant No. 2018YFC0407105]; National Natural Science Foundation of China (General Program) [Grant No. 51779154]; National Natural Science Foundation of China (General Program) [Grant No. 51979176].

Funding This work was supported by the research fund at Nanjing Hydraulic Research Institute.

Declarations

Conflicts of interest The authors declare that they have no conflicts of interest.

References

- Askarinejad A, Akca D, Springman SM (2018) Precursors of instability in a natural slope due to rainfall: a full-scale experiment. *Landslides* 15(3):1745–1759. <https://doi.org/10.1007/s10346-018-0994-0>
- Bondur VG, Zakharova LN, Zakharov AI et al (2019) Monitoring of landslide processes by means of l-band radar interferometric observations: Bureya river bank caving case. *Issledovanie Zemli Iz Kosmosa* 5:3–14. <https://doi.org/10.31857/S0205-9614201953-14>
- Boyages CS (2013) Global climate change, geo-engineering and human health. *Med J Aust* 199(7):501–502. <https://doi.org/10.5694/mja13.10572>
- Brezzi L, Bossi G, Gabrieli F et al (2016) A new data assimilation procedure to develop a debris flow run-out model. *Landslides* 13(5):1083–1096. <https://doi.org/10.1007/s10346-015-0625-y>
- Bui HH, Fukagawa R, Sako K et al (2010) Lagrangian meshfree particles method (SPH) for large deformation and failure flows of geomaterial using elastic-plastic soil constitutive model. *Int J Numer Anal Meth Geomech* 32(12):1537–1570. <https://doi.org/10.1002/nag.688>
- Calvo L, Haddad B, Pastor M et al (2015) Runout and deposit morphology of Bingham fluid as a function of initial volume: implication for debris flow modelling. *Nat Hazards* 75(1):489–513. <https://doi.org/10.1007/s11069-014-1334-x>
- Dai Z, Wang F, Yang H et al (2020) Numerical investigation on the kinetic characteristics of the Yigong landslide in Tibet. China. <https://doi.org/10.5194/nhess-2020-289>
- Frigaard IA, Nour C (2005) On the usage of viscosity regularisation methods for visco-plastic fluid flow computation. *J Nonnewton Fluid Mech* 127(1):1–26. <https://doi.org/10.1016/j.jnnfm.2005.01.003>
- Huang Y, Zhu C (2014) Simulation of flow slides in municipal solid waste dumps using a modified MPS method[J]. *Nat Hazards* 74(2):491–508. <https://doi.org/10.1007/s11069-014-1194-4>
- Huang Y, Dai Z, Zhang W et al (2013) SPH-based numerical simulations of flow slides in municipal solid waste landfills[J]. *Waste Manage Res* 31(3):256–264. <https://doi.org/10.1177/0734242X12470205>
- Hwang JY, Ohnishi Y, Wu J (2004) Numerical analysis of discontinuous rock masses using three-dimensional discontinuous deformation analysis (3D DDA). *KSCE J Civ Eng* 8(5):491–496. <https://doi.org/10.1007/BF02899576>
- Kang C, Chan D, Su F et al (2017) Runout and entrainment analysis of an extremely large rock avalanche—a case study of Yigong, Tibet. China *Landslides* 14(1):123–139. <https://doi.org/10.1007/s10346-016-0677-7>
- Kaya A, İmit Murat MDLL. (2020) Slope stability evaluation and monitoring of a landslide: a case study from NE Turkey. *J Mt Sci* 17(11):2624–2635. <https://doi.org/10.1007/s11629-020-6306-x>
- Keqiang H, Xiangran L, Xueqing Y et al (2008) The landslides in the three Gorges reservoir region, China and the effects of water storage and rain on their stability. *Environ Geol* 55(1):55–63. <https://doi.org/10.1007/s00254-007-0964-7>
- Koshizuka S, Nobe A, Oka Y (2015) Numerical analysis of breaking waves using the moving particle semi-implicit method[J]. *Int J Numer Meth Fluids* 26(7):751–769. [https://doi.org/10.1002/\(SICI\)1097-0363\(19980415\)26:7%3c751::AID-FLD671%3e3.0.CO;2-C](https://doi.org/10.1002/(SICI)1097-0363(19980415)26:7%3c751::AID-FLD671%3e3.0.CO;2-C)
- Kwok CY, Bolton MD (2013) DEM simulations of soil creep due to particle crushing. *Geotechnique* 63(16):1365–1376. <https://doi.org/10.1680/geot.11.P.089>
- Li X, Xie Y, Gutierrez M (2018) A soft-rigid contact model of MPM for granular flow impact on retaining structures. *Computational Particle Mechanics* 5(4):529–537. <https://doi.org/10.1007/s40571-018-0188-5>

- Li P, Shen W, Hou X et al (2019a) Numerical simulation of the propagation process of a rapid flow-like landslide considering bed entrainment: A case study. *Eng Geol* 263:105287. <https://doi.org/10.1016/j.enggeo.2019.105287>
- Li Q, Lu Y, Wang Y et al (2019b) Debris flow risk assessment based on a water-soil process model at the watershed scale under climate change: a case study in a debris-flow-prone area of southwest China. *Sustainability* 11(11):3199. <https://doi.org/10.3390/su11113199>
- Liang L, Wang Y (2020) Identification of failure slip surfaces for landslide risk assessment using smoothed particle hydrodynamics. *Georisk: Assess Manag Risk Eng Syst Geohazards* 14(2):91–111. <https://doi.org/10.1080/17499518.2019.1602877>
- Liu MB, Liu GR, Zong Z (2008) An overview on smoothed particle hydrodynamics. *Int J Comput Methods* 5(1):135–188. <https://doi.org/10.1142/S021987620800142X>
- Lucy LB (1997) A numerical approach to the testing of the fission hypothesis. *Astrophys J* 8(12):1013–1024. <https://doi.org/10.1086/112164>
- Ma C, Deng J, Wang R (2018) Analysis of the triggering conditions and erosion of a runoff-triggered debris flow in Miyun County, Beijing. *China Landslides* 15(12):2475–2485. <https://doi.org/10.1007/s10346-018-1080-3>
- Manzanal D, Drempevic V, Haddad B et al (2016) Application of a new rheological model to rock avalanches: An SPH approach. *Rock Mech Rock Eng* 49(6):1–20. <https://doi.org/10.1007/s00603-015-0909-5>
- Nohara S, Suenaga H, Nakamura K (2018) Large deformation simulations of geomaterials using moving particle semi-implicit method. *J Rock Mech Geotech Eng* 10(06):118–128. <https://doi.org/10.1016/j.jrmge.2018.06.005>
- Ouyang C, An H, Zhou S et al (2019) Insights from the failure and dynamic characteristics of two sequential landslides at Baige village along the Jinsha River. *China Landslides* 16(7):1397–1414. <https://doi.org/10.1007/s10346-019-01177-9>
- Papanastasiou TC (1987) Flows of materials with yield. *J Rheol* 31(5):385–404. <https://doi.org/10.1122/1.549926>
- Pastor M, Manzanal D, Merodo JAF et al (2010) From solids to fluidized soils: diffuse failure mechanisms in geostructures with applications to fast catastrophic landslides. *Granular Matter* 12(3):211–228. <https://doi.org/10.1007/s10035-009-0152-4>
- Pastor M, Blanc T, Haddad B et al (2014) Application of a SPH depth-integrated model to landslide run-out analysis. *Landslides* 11(5):793–812. <https://doi.org/10.1007/s10346-014-0484-y>
- Pastor M, Blanc T, Haddad B et al (2015a) Depth Averaged models for fast landslide propagation: mathematical, rheological and numerical aspects. *Arch Comput Methods Eng* 22(1):1–38. <https://doi.org/10.1007/s11831-014-9110-3>
- Pastor M, Stickle MM, Dutto P et al (2015b) A viscoplastic approach to the behaviour of fluidized geomaterials with application to fast landslides. *Continuum Mech Thermodyn* 27(1–2):21–47. <https://doi.org/10.1007/s00161-013-0326-5>
- Rangari VA, Umamahesh NV, Patel AK (2021) Flood-hazard risk classification and mapping for urban catchment under different climate change scenarios: a case study of Hyderabad city. *Urban Climate* 36(2015):100793. <https://doi.org/10.1016/j.uclim.2021.100793>
- Shen W, Wang D, Qu H et al (2019) The effect of check dams on the dynamic and bed entrainment processes of debris flows. *Landslides* 16(11):2201–2217. <https://doi.org/10.1007/s10346-019-01230-7>
- Soga K, Alonso E, Yerro A et al (2016) Trends in large-deformation analysis of landslide mass movements with particular emphasis on the material point method. *Géotechnique* 66(3):1–26. <https://doi.org/10.1680/jgeot.15.LM.005>
- Sulsky D, Chen Z, Schreyer HL (1994) Particle method for history-dependent materials. *Comput Methods Appl Mech Eng* 118(1–2):179–196. [https://doi.org/10.1016/0045-7825\(94\)90112-0](https://doi.org/10.1016/0045-7825(94)90112-0)
- Tang K, Wang J, Li L (2020) A prediction method based on monte carlo simulations for finite element analysis of soil medium considering spatial variability in soil parameters. *Adv Mater Sci Eng* 11:1–10. <https://doi.org/10.1155/2020/7064640>
- Tayyebi SM, Pastor M, Yifru AL, et al. (2021) Depth integrated two-layer coupled sph models for debris flows simulation. In: International conference of the international association for computer methods and advances in geomechanics. Springer, Cham. doi: https://doi.org/10.1007/978-3-030-64518-2_58
- Wang K, Zhang S (2021) Rainfall-induced landslides assessment in the Fengjie County, three-Gorge reservoir area. *China Natural Hazards* 11:1–28. <https://doi.org/10.1007/s11069-021-04691-z>
- Wang L, Yin Y, Huang B et al (2019) Damage evolution and stability analysis of the Jianchuandong dangerous rock mass in the three gorges reservoir area. *Eng Geol* 265:105439. <https://doi.org/10.1016/j.enggeo.2019.105439>

- Xing X, Wu C, Li J et al (2021) Susceptibility assessment for rainfall-induced landslides using a revised logistic regression method. *Nat Hazards* 106(1):97–117. <https://doi.org/10.1007/s11069-020-04452-4>
- Xiong J, Tang C, Chen M et al (2021) Activity characteristics and enlightenment of the debris flow triggered by the rainstorm on 20 August 2019 in Wenchuan County, China. *Bull Eng Geol Env* 80(2):873–888. <https://doi.org/10.1007/s10064-020-01981-x>
- Xu WJ, Wang YJ, Dong XY (2021) Influence of reservoir water level variations on slope stability and evaluation of landslide tsunami. *Bull Eng Geol Env* 80(6):4891–4907. <https://doi.org/10.1007/s10064-021-02218-1>
- Yu Y, Ren X, Zhang J et al (2020) Seepage, deformation, and stability analysis of sandy and clay slopes with different permeability anisotropy characteristics affected by reservoir water level fluctuations. *Water* 12(1):201. <https://doi.org/10.3390/w12010201>
- Yu S, Ren X, Zhang J et al (2021) An improved form of smoothed particle hydrodynamics method for crack propagation simulation applied in rock mechanics. *Int J Min Sci Technol* 31(3):421–428. <https://doi.org/10.1016/j.ijmst.2021.01.009>
- Zhang Y, Zhu S, Zhang W et al (2019) Analysis of deformation characteristics and stability mechanisms of typical landslide mass based on the field monitoring in the Three Gorges Reservoir. *China J Earth Syst Sci* 128(1):9. <https://doi.org/10.1007/s12040-018-1036-y>
- Zhang Y, Zhang Z, Xue S et al (2020) Stability analysis of a typical landslide mass in the three gorges reservoir under varying reservoir water levels. *Environmental Earth Sciences* 79(1):42. <https://doi.org/10.1007/s12665-019-8779-x>
- Zhu C, Huang Y, Zhan LT (2018) SPH-based simulation of flow process of a landslide at Hongao landfill in China[J]. *Nat Hazards* 93(3):1113–1126. <https://doi.org/10.1007/s11069-018-3342-8>
- Zhu HX, Yin ZY, Zhang Q (2020) A novel coupled FDM-DEM modelling method for flexible membrane boundary in laboratory tests. *Int J Numer Anal Meth Geomech* 44(3):389–404. <https://doi.org/10.1002/nag.3019>
- Zhu C, Chen Z, Huang Y (2021) Coupled moving particle simulation-finite-element method analysis of fluid-structure interaction in geodisasters. *Int J Geomech* 21(6):04021081. [https://doi.org/10.1061/\(ASCE\)GM.1943-5622.0002041](https://doi.org/10.1061/(ASCE)GM.1943-5622.0002041)

Publisher's Note Springer Nature remains neutral with regard to jurisdictional claims in published maps and institutional affiliations.